https://doi.org/10.3311/PPme.37299

Periodica Polytechnica Mechanical Engineering

Sono-hydrogen: a Theoretical Investigation of its Energy Intensity

Ahmad Al-Awamleh[1], Ferenc Hegedűs[1*]

[1] Department of Hydrodynamic Systems, Faculty of Mechanical Engineering, Budapest University of Technology and Economics, H- 1521, Budapest, P.O.B. 91., Hungary
[*] Corresponding author, e-mail: fhegedus@hds.bme.hu

Received: 09 May 2024, Accepted: 27 May 2024, Published online: 24 June 2024

Abstract

The present paper investigates the energy efficiency of hydrogen production by a freely oscillating microbubble placed in an infinite domain of liquid water. The spherical bubble initially contains a mixture of argon and water vapour. The bubble is expanded from its equilibrium size to a specific maximum radius via an isothermal expansion. The work needed to expand the bubble is its potential energy calculated by the sum of the work done by the internal gas, the work needed to displace the mass of the surrounding liquid, and the work needed to increase the area of the bubble against the surface tension. During the radial pulsation of the freely oscillating bubble, the internal temperature can reach several thousands of degrees of Kelvin inducing chemical reactions. The chemical yield is computed by solving a set of ordinary differential equations describing the radial dynamics of the bubble (Keller—Miksis equations), the temporal evolution of the internal temperature (first law of thermodynamics), and the concentration of the chemical species (reaction mechanism). The control parameters during the simulations were the equilibrium bubble size, initial expansion ratio, ambient pressure and temperature, the accommodation coefficient of the evaporation/condensation and the surface tension. In the best-case scenario, the energy requirement is 4072.3 MJ/kg.

Keywords

hydrogen production, sono-hydrogen, bubble dynamics, microbubbles, energy efficiency

1 Introduction

The transformation towards clean energy is required to achieve net-zero emissions, which has become significant more than ever for addressing global warming and air pollution [1]. Hydrogen might play a vital role in attaining this goal as it is a sustainable energy carrier having zero greenhouse gas emissions and the highest thermal energy of all fuels [2]. However, the method by which hydrogen is generated determines its impact on the environment [2]. For its production, various technologies exist such as the widely used steam reforming, gasification, and partial oxidization [3–5]. Despite being efficient, they are unsustainable and have detrimental impacts on the environment [6].

Thus, several clean technologies were developed: water electrolysis, photocatalysis, biophotolysis, and photobiological processes to name a few [4, 5]. While water electrolysis produces very pure hydrogen, it is energy-intensive as it requires 48 kWh to produce one kg of hydrogen (180 MJ/kg). Nevertheless, it can be combined with renewable energy sources such as solar, wind, hydro or even nuclear power. New difficulties, however, emerge concerning using and storing the excess energy, system operation, and energy supply reliability [7].

In recent times, producing hydrogen via sonochemistry (sono-hydrogen) has become the focus of many researchers. It is well-known that transmitting high-intensity and high-frequency acoustic waves in a liquid medium leads to the production of numerous microbubbles in a phenomenon called acoustic cavitation [8]. These micron-sized bubbles, containing water vapor and dissolved gases, start to pulsate around their equilibrium radii in successive expansion and implosion phases, rendering them to micro-reactors of extreme temperatures and pressures (thousands of degrees of Kelvin and hundreds of bars). This leads to the dissociation of water vapor trapped inside the bubble into hydrogen and oxidants [9]. Sonoluminescence [10, 11] is a direct experimental proof for the existence of such extreme conditions.

Numerous studies investigated the impact of dissolved gases and operational parameters (e.g., ultrasonic frequency,

Cite this article as: Al-Awamleh, A., Hegedűs, F. "Sono-hydrogen: a Theoretical Investigation of its Energy Intensity", Periodica Polytechnica Mechanical Engineering, 2024. https://doi.org/10.3311/PPme.37299

acoustic amplitude, static pressure, and liquid temperature) on H_2 yielding [9, 12–16]. Merouani et al. [9] performed numerical simulations examining the influence of several control parameters, namely ultrasonic frequency, acoustic intensity, and liquid temperature. They found that the production rate of hydrogen decreases considerably as the frequency increases due to the reduced compression ratio. An optimum liquid temperature (30 °C) was also shown to exist and it was attributed to the bubble temperature and water vapor content entrapped inside the bubble rather than its dynamics. Dehane et al. [13] investigated numerically the influence of some noble gases (Ar, Xe, and He) on sono-hydrogen at different frequencies (213 – 515 kHz) and acoustic intensities (1 – 2). Ar and Xe proved their efficiency as saturating gases due to their lower thermal diffusivity and higher heat capacity, whereas the inefficiency of He was confirmed for the sonochemical production of hydrogen.

Although hydrogen production by ultrasound is possible, only a few papers attempted to examine the energy efficiency of the process [14, 17, 18]. Rashwan et al. [18] investigated the energy required to produce 1 μmol of hydrogen under only a single parameter combination, i.e., an acoustic frequency and amplitude of 20 kHz and 2.6 atm, respectively. Assuming that the number of bubbles is known from the experimental work of Petrier and Francony [19] and Jiang et al. [20], Rashwan et al. [18] reported an energy efficiency of 0.15 μmol/kWh (1.19×10^{10} MJ/kg). However, in a real sono-reactor, determining the number of active bubbles is a highly complex task and the millions of bubbles have complex interactions via hydrodynamic and acoustic (Bjerknes) forces [21], possibly leading to a non-spherical collapse, bubble coalescence, or acoustic shielding [22–27]. In addition, the bubble cluster has a size distribution and the yields of the bubbles are not identical; thus, approximating the sonoreactor yield through the multiplication of a single-bubble yield by the number of bubbles leads to an inaccurate estimation of H_2 energy intensity.

Due to the aforementioned inconsistency, in this paper, we adopted a single-bubble approach for the assessment of the energy efficiency of sono-hydrogen in large-scale high-resolution parametric studies, accounting for the most important control parameters affecting its production: the ambient radius, static pressure, water temperature, accommodation coefficient of phase change and surface tension. The energy requirement is computed by the maximum potential energy of the bubble, whereas the hydrogen yield is obtained by solving the complex reaction kinetics inside the bubble. Therefore, the input energy and chemical yield are consistent, and a comparison can be made between the energy intensity of sono-hydrogen with that of water electrolysis to decide whether sono-hydrogen could be a viable alternative technology for producing hydrogen.

A simplified test case is employed to be able to calculate the theoretical energy requirement (potential energy) precisely. First, an equilibrium bubble size is specified filled with non-reactive argon gas and water vapor under equilibrium conditions. Second, the bubble is initially expanded isothermally up to a maximum radius, where the potential energy can be obtained analytically. Third, the bubble is released and start to oscillate freely. Typically, during the first collapse phase, chemical reactions and water vapor dissociation take place. The main products after the rebound are hydrogen and oxygen. Such a simplified scenario can serve as a baseline for the energy intensity of hydrogen production by microbubbles.

2 The governing equations

The mathematical model of a single bubble consists of two parts: physical and chemical. The physical model describes the bubble dynamics, whereas the chemical model deals with bubble chemistry. Our improved chemical model uses up-to-date Arrhenius constants and third-body efficiencies. It also accounts for reaction duplication and pressure-dependency of the reactions. These chemical modeling issues are not considered in the sonochemical literature resulting in several orders of magnitude differences in the chemical yields as detailed in our previous paper [28].

The bubble and its interior are assumed to be spherically symmetric and spatially uniform. In the following, we briefly describe the employed mathematical model; for a complete description, the reader is referred to [21, 28]. The radial oscillation of the bubble is described by the modified Keller—Miksis equation [29]:

$$\left(1-\frac{\dot{R}}{c_L}\right)\cdot R\cdot\ddot{R}+\left(1-\frac{\dot{R}}{c_L}\right)\cdot\frac{3}{2}\cdot\dot{R}^2 = \left(1+\frac{\dot{R}}{c_L}+\frac{R}{c_L}\cdot\frac{d}{dt}\right)\cdot\frac{\left(p_L\left(R,t\right)-p_\infty\left(t\right)\right)}{\rho_L}, \tag{1}$$

where the dot denotes the temporal derivative. The material properties c_L, ρ_L, μ_L and σ are the liquid sound speed, density, viscosity and surface tension, respectively. For a non-excited bubble, the ambient static pressure $p_\infty(t) = p_\infty$ is constant. The pressure of the gas mixture is determined via the ideal gas law

$$p = M\ R_g\ T, \tag{2}$$

where M and R_g are the total concentration and the universal gas constant of the mixture, respectively. The internal temperature T is computed according to the first law of thermodynamics:

$$\dot{T} = \frac{-p\dot{V} + \sum \dot{Q}}{n_t \bar{C}_v} \tag{3}$$

Here, $V = 4 \cdot R^3 \cdot \pi/3$ denotes the bubble volume and $\sum \dot{Q}$ represents the sum of reaction heat and heat diffusion. The heat conduction between the bubble interior and the liquid medium is modeled by the approach of Toegel et al. [30]. In addition, n_t and $\bar{C}_v$ are the total number of moles and the average molar heat capacity at constant volume, respectively.

2.1 Brief description of the reaction mechanism

As for the chemical kinetics, the production rate of component k is expressed as:

$$\dot{\omega}_k = \sum_{i=1}^{I} \nu_{ki} \cdot q_i, \tag{4}$$

where q_i denotes the net reaction rate of the i^{th} reaction and ν_{ki} are the stoichiometric coefficients. This net reaction rate is determined as:

$$q_i = k_{f_i} \cdot \prod_{k=1}^{K} c_k^{\nu_{ki}^f} - k_{b_i}, \tag{5}$$

where k_{fi} and k_{bi} are the forward and backward reaction rate constants of reaction i, respectively; c_k is the concentration of component k, $K = 10$ is number of chemical species; and ν^f_{ki} and ν^b_{ki} are the forward and backward stoichiometric coefficients, respectively. The dependence of the forward rate coefficient k_f on temperature is expressed by the Arrhenius-equation as:

$$k_{f_i} = A_i \cdot T^{b_i} \cdot \exp\left(\frac{-E_i}{R_g \cdot T}\right), \tag{6}$$

where A_i, b_i and E_i are the pre-exponential factor, temperature exponent and activation energy, respectively. As shown in [28], this (forward) reaction rate is modified in case of pressure-dependent, duplicated, and third-body reactions. The backward reaction rates are computed via thermodynamic equilibrium conditions, for the details the reader is again referred to [28].

2.2 The Structure of the governing equations

In summary, the ordinary differential equation (ODE) system has the following structure. The Keller—Miksis equation is reduced to two first-order equations describing the temporal evolution of the bubble radius R and the bubble wall velocity $\dot{R}$. In our chemical mechanism, there are ten chemical components (K = 10), and their concentrations are governed by:

$$\dot{c}_k = \dot{\omega}_k - c_k \cdot \frac{\dot{V}}{V} \tag{7}$$

Finally, the bubble temperature is estimated by using the first law of thermodynamics. Combining these ODEs, a set of $K + 3$ equations is obtained in which two describe the bubble dynamics, one provides the bubble temperature, and ten equations quantify the concentrations.

3 Control parameters and the numerical technique

Due to the stiffness of the ODE system, two Python-based solvers were used: LSODA and Radau. LSODA can detect the stiffness and select automatically between the non-stiff Adams and stiff BDF techniques, whereas Radau is an implicit method of the Radau IIA family of order five suitable for stiff problems [31]. The solution technique employed is as follows: since LSODA is faster and can be a good universal choice for solving a system of ODEs, LSODA attempts first to solve the bubble model for 30 s. If it fails, Radau tries to solve it for 300 s.

Two solution/visualization strategies are applied in the paper. First, a pattern search algorithm is implemented to seek optimal parameter combinations in the parameter ranges provided in Table 1. This is key to optimizing energy intensity in a high dimensional parameter space. Second, high-resolution bi-parametric maps are created around the obtained optimal parameter combinations to examine their sensitivity.

Table 1 General overview of the control parameters and their employed ranges and resolutions

parameter	symbol	range	resolution
expansion ratio	$\frac{R_0}{R_E}[-]$	2 – 20	101 (log scale)
equilibrium radius	R_E [μm]	0.1 – 20	101 (log scale)
ambient pressure	P_∞ [*bar*]	1 – 300	–
ambient temperature	T_∞ [°C]	5 – 100	–
accommodation coefficient	α [–]	0 – 0.35	0.05
surface tension	$\sigma\left[\frac{N}{m}\right]$	0 – 0.072	–

The investigated control parameters, their ranges and resolutions are provided in Table 1. If resolution is not specified, the corresponding parameter is employed only during the pattern search optimum finding algorithm. The impact of the parameters on the energy intensity of hydrogen production is briefly introduced here. The first key parameter is the bubble radius, which is related to the initial amount of water vapor present in the bubble. The larger the bubble is, the larger the hydrogen yield might be. The initial expansion ratio is also considered a main parameter since it determines the potential energy and influences the first collapse strength which in turn affects H_2 yield. From the perspective of the input energy during expansion, surface tension (controlled, e.g., via surfactants [32]) and static pressure are worth investigating since they work against bubble expansion. In addition, the accommodation coefficient describes the evaporation and condensation of water vapor. The last parameter, the water temperature, determines the vapor pressure and impacts H_2 yield by affecting the H_2O content in the bubble.

4 Definition of the energy intensity and chemical yield

Fig. 1 shows a typical time series curve of a freely oscillating bubble to demonstrate the computation of the energy intensity. In the top panel, the time evolutions of the bubble radius and internal temperature are plotted. The equilibrium radius is 1.7 μm and the static pressure and water temperature are 1 bar and 25 °C, respectively. Initially, the bubble radius (blue curve) rapidly compresses from its initial size due to liquid inertia, and the internal temperature (red curve) reaches as high as 8000 K at the end of the first collapse. Then the bubble loses most of its energy via acoustic emission and experiences a decaying oscillation approaching to its equilibrium radius. In the lower panel, the evolution of the chemical species in moles is shown on a logarithmic scale. The bubble is initially filled with argon and water vapor. During the compression phase, water vapor concentration decreases as it dissociates to hydrogen and other chemical species or condenses to liquid water. This is indicated by the increase in the concentrations of various chemical species at the end of the first collapse. Note that the hydrogen yield remains unchanged after the first collapse. Observe also the orders of magnitude differences between the yields of hydrogen and other chemical species.

The potential energy W_P is the energy required to expand the bubble from R_E to $R_{\max}$ expressed as:

$$W_P = W_G + W_A + W_L, \tag{8}$$

where, W_g is the work done by the expanding gas. Assuming isothermal (slow) expansion it is written as:

$$W_G = -N_{t,0} \cdot R_g \cdot T_\infty \cdot \ln\left(\frac{R_{\max}^3}{R_E^3}\right), \tag{9}$$

in which $N_{t,0}$ and T_∞ are the total number of moles in the bubble and the ambient temperature, respectively. The quantities W_A and W_L are the energies required to enlarge the bubble against surface tension and the surrounding liquid. They read as:

$$W_A = \sigma \cdot 4 \cdot \pi \cdot \left(R_{\max}^2 - R_E^2\right), \tag{10}$$

and

$$W_L = P_\infty \cdot \frac{4 \cdot \pi}{3} \cdot \left(R_{\max}^3 - R_E^3\right). \tag{11}$$

Here, $R_{\max}$ and P_∞, are the largest radius to which the bubble expands and the ambient static pressure, respectively. Finally, in our analysis, the energy intensity (in terms of MJ/kg) is computed as follows:

$$E = W_P / n_{H_2} M_{H_2}, \tag{12}$$

where M_{H_2} and n_{H_2} are the molar mass of hydrogen and the generated hydrogen in moles, respectively. The produced hydrogen is obtained by reading its value at the end of the simulation, where the equilibrium conditions reached (zero bubble wall velocity), see again the bottom panel of Fig. 1. This efficiency assessment approach makes it possible to estimate the minimum achievable theoretical energy intensity since it directly connects the minimum energy requirement to expand the bubble (potential energy) and the mass of produced hydrogen (chemical yield).

5 Optimization of energy efficiency

This section demonstrates the dependence of the energy intensity of hydrogen production on the six parameters. Due to the significant impact of the bubble radius and expansion ratio discussed earlier on the energy intensity of hydrogen production, a high-resolution map in the equilibrium radius and expansion ratio parameter plane is thus created at standard ambient conditions to optimize the energy intensity. This computation serves as a baseline compared to the literature data. Seeking lower optimal energy intensity values, the influence of ambient

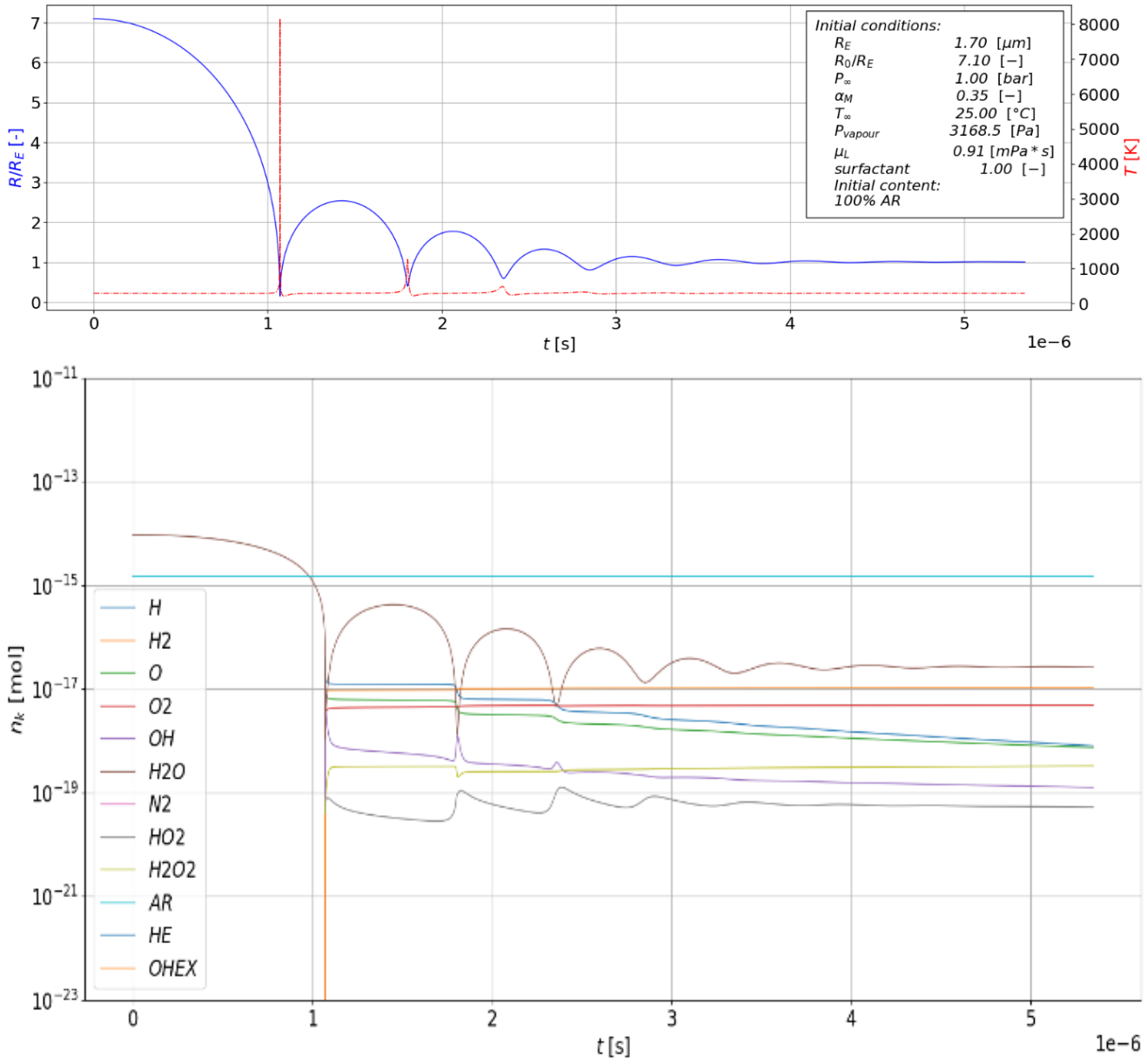

Fig. 1 A typical example of the dynamics of a freely oscillating microbubble. Top panel: bubble radius (blue) and internal temperature (red) as a function of time. Bottom panel: temporal evolution of the chemical species in moles.

properties, accommodation coefficient, and surface tension are then investigated using extensively the gradient descent algorithm due to the high-dimensional parameter space. This provides only the optimal conditions as a function of the studied control parameter.

5.1 Energy intensity at standard conditions

The influence of the equilibrium radius and expansion ratio on the energy efficiency is shown in Fig. 2 at a static ambient pressure of 1 bar and at a water temperature of 25 °C. The accommodation coefficient and the surface tension are set to 0.35 and 0.072, respectively. These are their upper limits, see Table 1. Investigating the chemical yield and energy intensity at a few parameter combinations might lead to false optimal operating conditions [25]; thus, the provided high-resolution contour plot provides an accurate scan of the optimal energy intensity. As shown in Fig. 2, the optimal energy intensity (red dot) is obtained at R_E = 1.7 μm and at R_0/R_E = 7.2 and turned out to be 38413 MJ/kg. This is 213 times higher than the energy requirement of hydrogen production via water electrolysis (180 MJ/kg).

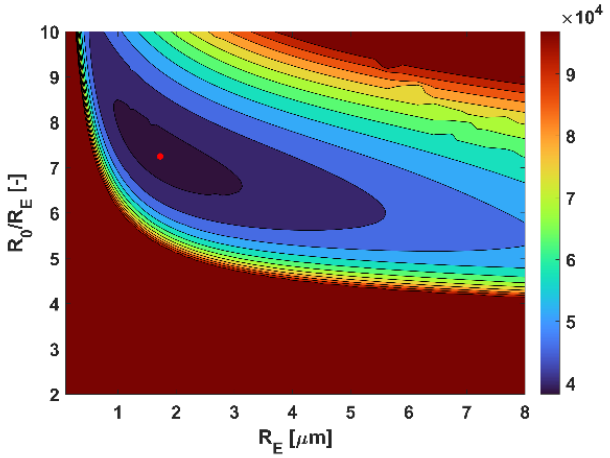

Fig. 2 Energy intensity of hydrogen production (in terms of MJ/kg) at 1 bar and 25 °C as a function of the bubble radius and expansion ratio. The dot represents the optimum parameter combination.

The results imply that the production of hydrogen via microbubbles has inferior energy intensity compared to water electrolysis. This is an important finding as sono-hydrogen literature is relatively large [9, 12–16], but energy intensity values are rarely provided or given in units like μmol/kWh that is hard to compare directly with the usual unit of MJ/kg. Although the values presented in this section are related to freely oscillating bubbles, they made it very clear that hydrogen production by microbubbles at standard conditions cannot be a viable alternative to water electrolysis.

5.2 Influence of the ambient properties

To reduce the energy requirement of sono-hydrogen obtained at standard conditions, the effect of the ambient conditions is also investigated. The accommodation coefficient and the surface tension are still set to 0.35 and 0.072. Performing an optimization in a four-dimensional parameter space, the optimum parameter combination is P_∞ = 198 bar, T_∞ = 87 °C, R_E = 0.49 μm and R_0/R_E = 4. The energy intensity is significantly reduced to 11192 MJ/kg which is "only" 63-fold higher than the energy efficiency of water electrolysis (180 MJ/kg). This suggests that by manipulating the radial dynamics, the energy intensity can significantly be improved. Before continuing with the extension of the parameter space and further optimizing the energy intensity, let us investigate the effect of the ambient properties in more details.

Fig. 3 provides three high-resolution contour plots at different ambient pressure-temperature combinations. From panels top to bottom, the ambient pressure is P_∞ = 20 bar, P_∞ = 198 bar and P_∞ = 300 bar, respectively. At each pressure value, an optimization procedure is performed to acquire the optimal ambient temperature values: T_∞ = 60 °C, T_∞ = 87 °C and T_∞ = 96 °C. The color code is the same as the one in Fig. 1. Similarly, the red dot depicts the optimum parameter combination in the equilibrium radius-expansion ratio parameter space.

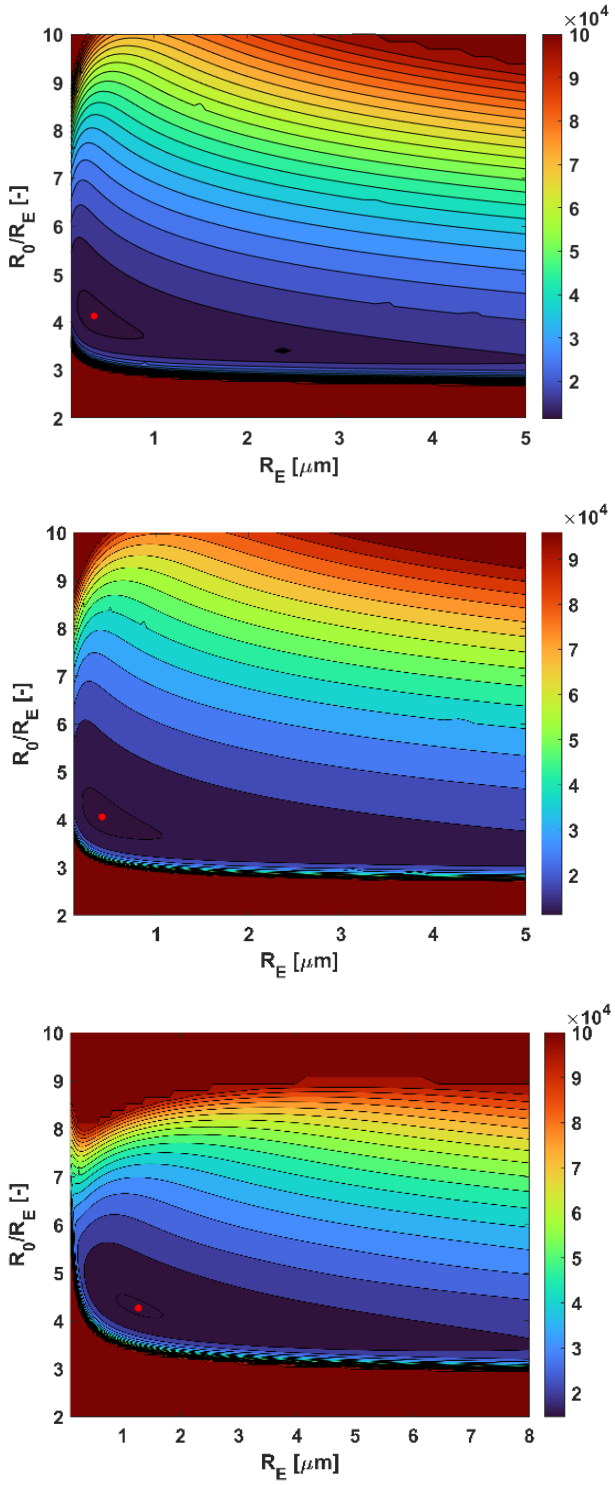

Fig. 3 Bi-parametric maps at different ambient properties. Top to down: 20 bar and 60 °C; 198 bar and 87 °C (optimal); and 300 bar and 96 °C.

Fig. 3 provides an insight into the energy intensity in a four-dimensional parameter space. Together with Fig. 2, it is clear that around the optimum point (red dot), there is a relatively large domain where the energy intensity does not increase significantly (dark blue regions). This means that the equilibrium bubble size and the expansion ratio do not need to be highly accurate. Thus, during an experiment, a relatively wide range of equilibrium radius is suitable.

To obtain an overview of the evolution of the optimal parameter setup as a function of the ambient pressure, a series of optimization problems are conducted at different pressure level values. The results are summarized in Fig. 4. The first panel shows the energy intensity curve. Its global minimum is in accordance with the optimum ambient pressure value P_∞ = 198 bar. The second panel depicts the corresponding optimum ambient temperatures. It increases monotonically with the ambient pressure. The third and fourth panels represent the optimal equilibrium bubble size and expansion ratio, respectively.

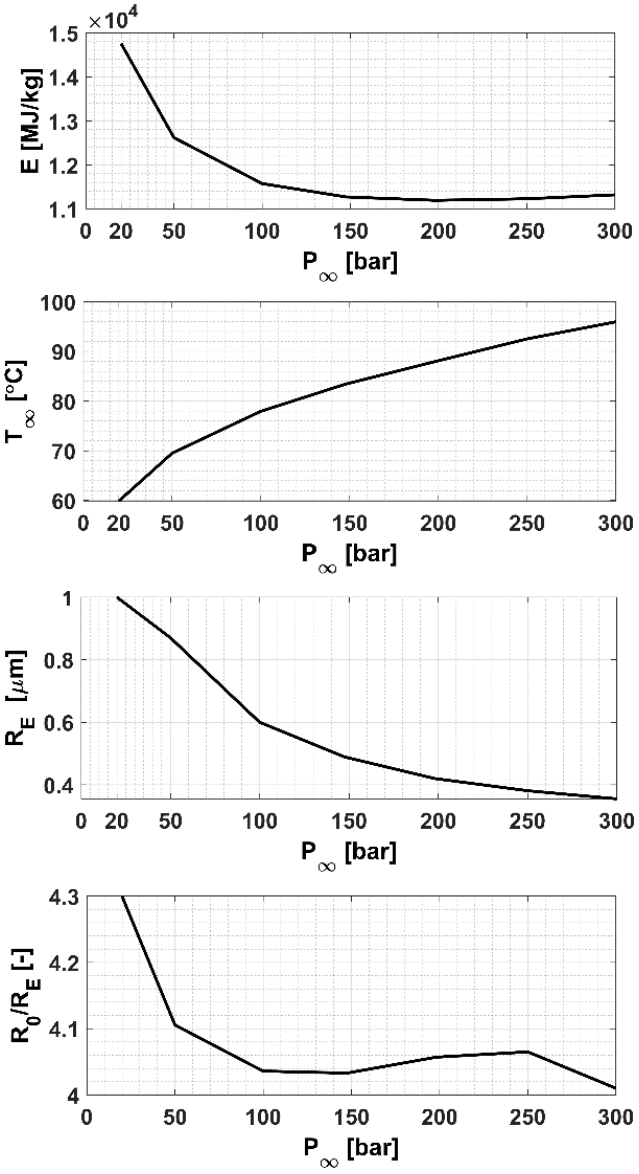

Fig. 4 Optimal energy intensity values and parameter combinations as a function of the ambient pressure

In general, it can be stated that the best-case scenario needs very small bubbles usually below micron size. This can be explained by the fact that the smaller the amount of non-reactive argon, the larger the amount of trapped water vapor that can be dissociated. Finally, although the expansion ratio varies in a complex manner, its value fluctuates in a relatively narrow range (approximately between 4 and 4.3).

5.3 The influence of the accommodation factor

During the previous computations, the accommodation coefficient was set to 0.35 based on the publication of Yasui [33]. Although this value is widely employed in the literature, it is well-known that the measured values are usually highly inconsistent and can vary between orders of magnitude [34]. In order to take into account such an uncertainty, the accommodation coefficient is treated as a free parameter, which is varied between 0.0 and 0.35 in steps of 0.05. Zero value means no water vapor condensation. This can be feasible for very fast bubble collapses where the water vapor has no time to diffuse to the bubble interface and condense. Fig. 5 presents a series of optimizations as a function of the accommodation coefficient . In a single simulation, the equilibrium size, expansion ratio, ambient pressure and temperature were the optimized parameters.

The top panel of Fig. 5 depicts the monotonic decrease of the energy intensity with decreasing accommodation coefficient. The energy intensity is reduced significantly to 4076.2 MJ/kg which is 23-fold higher compared to that of water electrolysis. This optimal case means no water condensation during the collapse. As mentioned before, such a scenario is valid only for a relatively fast collapse, and can serve as a good theoretical estimation for the achievable energy intensity limitations. Although the energy intensity value of 4076.2 MJ/kg is still highly uncompetitive, it represents a significant improvement and suggests that different physical conditions significantly influence the energy intensity.

The second, third, fourth and fifth panels of Fig. 5 represent the optimum of the ambient pressure, ambient temperature, expansion ratio and equilibrium size, respectively. With decreasing α, the ambient pressure and temperature, and the expansion ratio have a decreasing tendency. In contrast, the bubble size increases significantly up to several microns.

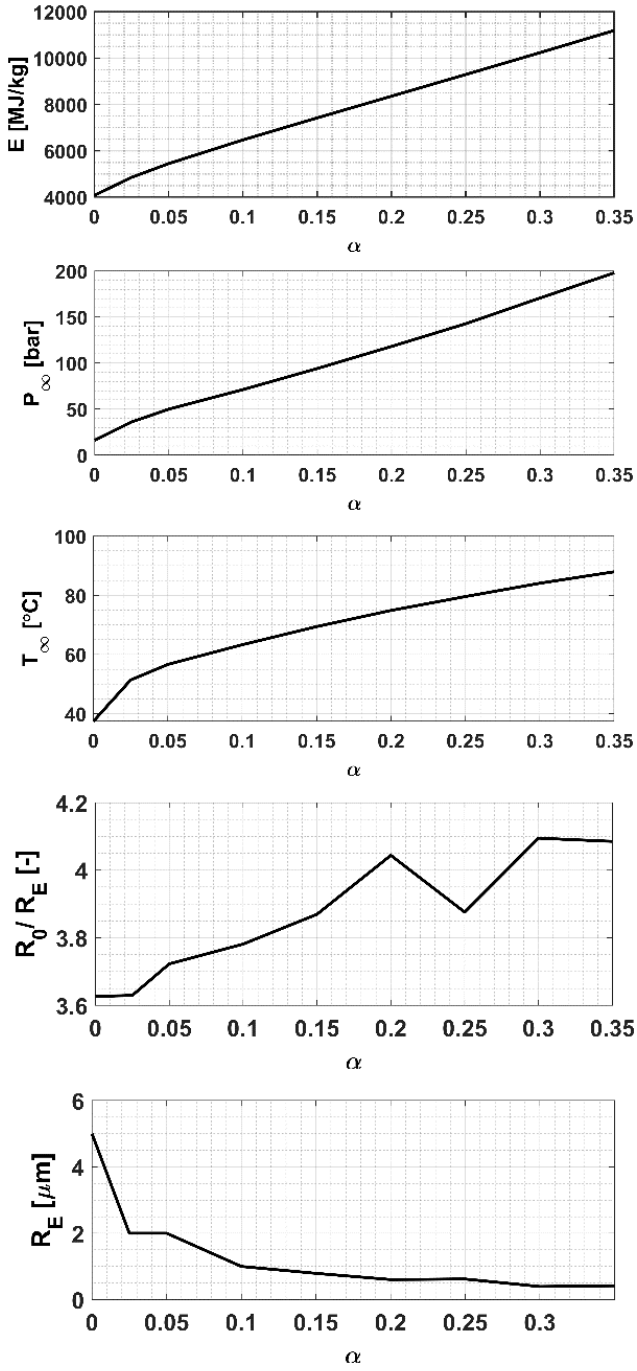

Fig. 5 The variation of the optimal control parameters as a function of the accommodation coefficient

5.4 The effect of surface tension

Suppressing the effects of surface tension and evaporation/condensation at the bubble wall ($\sigma = 0$ and $\alpha = 0$), the absolute optimal energy efficiency is marginally reduced to 4072.3 MJ/kg compared to 4076.2 MJ/kg obtained at $\sigma = 0.072$ N/m and $\alpha = 0$. The surface tension, therefore, has a marginal impact on the energy intensity of sono-hydrogen.

6 Discussion and summary

The main aim of the present study was to investigate the theoretical energy efficiency of hydrogen production via a freely oscillating bubble initially containing water vapor and argon. The input work is computed as the potential energy of the initially expanded bubble. The chemical yield is obtained via numerical simulations of the chemical history of the bubble. The control parameters were the equilibrium size of the bubble, initial expansion ratio, ambient pressure, ambient temperature, accommodation coefficient, and surface tension. At the best parameter combination, the energy intensity of hydrogen production was 4072.3 MJ/kg. In comparison, the energy requirement of the water electrolysis is 180 MJ/kg.

Although the energy intensity of sono-hydrogen is approximately 23 times higher than the water electrolysis technology, it is still several orders of magnitude better than the available data in the literature [18], keep in mind the indicated 1.19×10^{19} MJ/kg value in the introduction. Moreover, when the bubble is sonicated, one might get a smaller energy demand since the excitation parameters (i.e., the frequency, acoustic amplitude, and phase shift) can significantly manipulate the bubble dynamics and chemical yields. Therefore, the present theoretical work showed that sono-hydrogen can still be a viable option; however, intensive optimization on the operating strategy is necessary.

From an experimental point of view, the optimal ambient pressure $P_\infty = 16.2$ bar and temperature $T_\infty = 37.4$ °C (at zero accommodation coefficient) does not represent a technique difficulty. The optimal bubble size $R_E = 5$ μm is also within the typical range of bubble size distribution in a typical reactor [35]. The corresponding expansion ratio $R_0/R_E = 3.6$ is moderate, during sonoluminescence experiments, the expansion ratio can reach even more than a hundred [10].

Acknowledgement

Project no. TKP-6-6/PALY-2021 has been implemented with the support provided by the Ministry of Culture and Innovation of Hungary from the National Research, Development and Innovation Fund, financed under the TKP2021-NVA funding scheme. This paper was also supported by the NVIDIA Corporation via the Academic Hardware Grants Program. The authors acknowledge the financial support of the Hungarian National Research, Development and Innovation Office via NKFIH grant OTKA FK142376.

References

[1] Azevedo, I., Bataille, C., Bistline, J., Clarke, L., Davis, S. "Net-zero emissions energy systems: what we know and do not know", Energy and Climate Change, 2, 100049, 2021. https://doi.org/10.1016/j.egycc.2021.100049

[2] Christopher, K., Dimitrios, R. "A review on exergy comparison of hydrogen production methods from renewable energy sources", Energy & Environmental Science, 5(5), pp. 6640–6651, 2012. https://doi.org/10.1039/C2EE01098D

[3] Merouani, S., Hamdaoui, O. "Correlations Between the Sonochemical Production Rate of Hydrogen and the Maximum Temperature and Pressure Reached in Acoustic Bubbles", Arabian Journal for Science and Engineering, 43, pp. 6109–6117, 2018. https://doi.org/10.1007/s13369-018-3266-3

[4] Dincer, I. "Green methods for hydrogen production", International Journal of Hydrogen Energy, 37(2), pp. 1954–1971, 2012. https://doi.org/10.1016/j.ijhydene.2011.03.173

[5] Rashwan, S. S., Dincer, I., Mohany, A., Pollet, B. G. "The Sono-Hydro-Gen process (Ultrasound induced hydrogen production): Challenges and opportunities", International Journal of Hydrogen Energy, 44(29), pp. 14500–14526, 2019. https://doi.org/10.1016/j.ijhydene.2019.04.115

[6] Akhlaghi, N., Najafpour-Darzi, G. "A comprehensive review on biological hydrogen production", International Journal of Hydrogen Energy, 45(43), pp. 22492–22512, 2020. https://doi.org/10.1016/j.ijhydene.2020.06.182

[7] Ursua, A., Gandia, L. M., Sanchis, P. "Hydrogen production from water electrolysis: current status and future trends", Proceedings of the IEEE, 100(2), pp. 410–426, 2011. https://doi.org/10.1109/JPROC.2011.2156750

[8] Merouani, S., Hamdaoui, O., Rezgui, Y., Guemini, M. "Theoretical Procedure for the Characterization of Acoustic Cavitation Bubbles", Acta Acustica United with Acustica, 100(5), pp. 823–833, 2014. https://doi.org/10.3813/AAA.918762

[9] Merouani, S., Hamdaoui, O., Rezgui, Y., Guemini, M. "Computational engineering study of hydrogen production via ultrasonic cavitation in water", International Journal of Hydrogen Energy, 41(2), pp. 832–844, 2016. https://doi.org/10.1016/j.ijhydene.2015.11.058

[10] Dellavale, D., Rechiman, L., Rosselló, J. M., Bonetto, F. J. "Upscaling energy concentration in multifrequency single-bubble sonoluminescence with strongly degassed sulfuric acid", Physical Review E, 86(1), 016320, 2012. https://doi.org/10.1103/PhysRevE.86.016320

[11] Rosselló, J. M., Dellavale, D., Bonetto, F. J. "Energy concentration and positional stability of sonoluminescent bubbles in sulfuric acid for different static pressures", Physical Review E, 88(3), 033026, 2013. https://doi.org/10.1103/PhysRevE.88.033026

[12] Kerboua, K., Merouani, S., Hamdaoui, O., Alghyamah, A., Islam, M. H., Hansen, H. E., Pollet, B. G. "How do dissolved gases affect the sonochemical process of hydrogen production? an overview of thermodynamic and mechanistic effects–on the "hot spot theory" ", Ultrasonics Sonochemistry, 72, 105422, 2021. https://doi.org/10.1016/j.ultsonch.2020.105422

[13] Dehane, A., Merouani, S., Chibani, A., Hamdaoui, O. "Clean hydrogen production by ultrasound (sonochemistry): The effect of noble gases", Current Research in Green and Sustainable Chemistry, 5, 100288, 2022. https://doi.org/10.1016/j.crgsc.2022.100288

[14] Kerboua, K., Hamdaoui, O., Islam, M. H., Alghyamah, A., Hansen, H. E., Pollet, B. G. "Low carbon ultrasonic production of alternate fuel: Operational and mechanistic concerns of the sonochemical process of hydrogen generation under various scenarios", International Journal of Hydrogen Energy, 46(53), pp. 26770–26787, 2021. https://doi.org/10.1016/j.ijhydene.2021.05.191

[15] Dehane, A., Merouani, S., Hamdaoui, O., Alghyamah, A. "A complete analysis of the effects of transfer phenomenons and reaction heats on sono-hydrogen production from reacting bubbles: Impact of ambient bubble size", International Journal of Hydrogen Energy, 46(36), pp. 18767–18779, (2021). https://doi.org/10.1016/j.ijhydene.2021.03.069

[16] Dehane, A., Merouani, S., Hamdaoui, O. "Theoretical investigation of the effect of ambient pressure on bubble sonochemistry: Special focus on hydrogen and reactive radicals production", Chemical Physics, 547, 111171, 2021. https://doi.org/10.1016/j.chemphys.2021.111171

[17] Rashwan, S. S., Dincer, I., Mohany, A. "An investigation of ultrasonic based hydrogen production", Energy, 205, 118006, 2020. https://doi.org/10.1016/j.energy.2020.118006

[18] Rashwan, S. S., Dincer, I., Mohany, A. "A unique study on the effect of dissolved gases and bubble temperatures on the ultrasonic hydrogen (sonohydrogen) production", International Journal of Hydrogen Energy, 45(41), pp. 20808–20819, 2020. https://doi.org/10.1016/j.ijhydene.2020.05.022

[19] Pétrier, C., Francony, A. "Ultrasonic waste-water treatment: incidence of ultrasonic frequency on the rate of phenol and carbon tetrachloride degradation", Ultrasonics Sonochemistry, 4(4), pp. 295–300, 1997. https://doi.org/10.1016/S1350-4177(97)00036-9

[20] Jiang, Y. , Petrier, C., Waite, T. D. "Sonolysis of 4-chlorophenol in aqueous solution: effects of substrate concentration, aqueous temperature and ultrasonic frequency", Ultrasonics Sonochemistry, 13(5), pp. 415–422, 2006. https://doi.org/10.1016/j.ultsonch.2005.07.003

[21] Rosselló, J. M., Dellavale, D., Bonetto, F. J. "Stable tridimensional bubble clusters in multi-bubble sonoluminescence (MBSL)", Ultrasonics Sonochemistry, 22, pp. 59–69, 2015. https://doi.org/10.1016/j.ultsonch.2014.06.003

[22] Hegedűs, F., Kalmár, C., Turányi, T., Zsély, I. G., Papp, M. "Sonochemical reactions, when, where and how: Modelling approach", In: Energy Aspects of Acoustic Cavitation and Sonochemistry, Elsevier, pp. 49–77, 2022. ISBN 978-0-323-91937-1 https://doi.org/10.1016/B978-0-323-91937-1.00013-X

[23] Lauterborn, W., Parlitz, U. "Methods of chaos physics and their application to acoustics", The Journal of the Acoustical Society of America, 84(6), pp. 1975–1993, 1988. https://doi.org/10.1121/1.397042

[24] Lauterborn, W., Holzfuss, J. "Acoustic chaos", International Journal of Bifurcation and Chaos, 1(01), pp. 13–26, 1991. https://doi.org/10.1142/S0218127491000038

[25] Klapcsik, K., Varga, R., Hegedűs, F. , "Bi-parametric topology of subharmonics of an asymmetric bubble oscillator at high dissipation rate: The exoskeleton, its internal structure and the missing fine substructure", Nonlinear Dynamics, 94, pp. 2373–2389, 2018. https://doi.org/10.1007/s11071-018-4497-2

[26] Sojahrood, A. J., Wegierak, D., Haghi, H., Karshfian, R. , Kolios, M. C. "A simple method to analyze the super-harmonic and ultra-harmonic behavior of the acoustically excited bubble oscillator", Ultrasonics Sonochemistry, 54, pp. 99–109, 2019. https://doi.org/10.1016/j.ultsonch.2019.02.010

[27] Sojahrood, A. J., Li, Q., Haghi, H., Karshafian, R., Porter, T. M., Kolios, M. C. "Towards the accurate characterization of the shell parameters of microbubbles based on attenuation and sound speed measurements", The Journal of the Acoustical Society of America, 141(5), 3493, 2017. https://doi.org/10.1121/1.4987297

[28] Kalmár, C., Turányi, T., Zsély, I. G., Papp, M., Hegedűs, F. "The importance of chemical mechanisms in sonochemical modelling", Ultrasonics Sonochemistry, 83, 105925, 2022. https://doi.org/10.1016/j.ultsonch.2022.105925

[29] Keller, J. B., Miksis, M. "Bubble oscillations of large amplitude", The Journal of the Acoustical Society of America, 68(2), pp. 628–633, 1980. https://doi.org/10.1121/1.384720

[30] Toegel, R., Gompf, B., Pecha, R., Lohse, D. "Does water vapor prevent upscaling sonoluminescence?", Physical Review Letters, 85(15), pp. 3165–3168, 2000. https://doi.org/10.1103/PhysRevLett.85.3165

[31] Wanner, G., Hairer, E. "Solving ordinary differential equations II", Springer Berlin Heidelberg, New York, 1996. ISBN 978-3-540-60452-5 https://doi.org/10.1007/978-3-642-05221-7

[32] Sostaric, J. Z., Riesz, P. "Sonochemistry of Surfactants in Aqueous Solutions: An EPR Spin-Trapping Study", Journal of American Chemical Society, 123(44), pp. 11010–11019, 2001. https://doi.org/10.1021/ja010857b

[33] Yasui, K., Tuziuti, T., Kozuka, T., Towata, A., Iida, Y. "Relationship between the bubble temperature and main oxidant created inside an air bubble under ultrasound", The Journal of Chemical Physics, 127(15), 154502, 2007. https://doi.org/10.1063/1.2790420

[34] Fujikawa, S., Yano, T., Watanabe, M. "Vapor-Liquid Interfaces, Bubbles and Droplets", Springer, 2011. ISBN 978-3-642-18037-8 https://doi.org/10.1007/978-3-642-18038-5

[35] Iida, Y. Ashokkumar, M., Tuziuti, T., Kozuka, T., Yasui, K., Towata, A., Lee, J. "Bubble population phenomena in sonochemical reactor: II. Estimation of bubble size distribution and its number density by simple coalescence model calculation", Ultrasonics Sonochemistry, 17(2), pp. 480–486, 2010. https://doi.org/10.1016/j.ultsonch.2009.08.017